International Advance Journal of Engineering, Science and Management (IAJESM)
Multidisciplinary, Indexed, Double Blind, Open Access, Peer-Reviewed, Refereed-International Journal.
SJIF Impact Factor =7.938, January-June 2024, Submitted in February 2024, ISSN -2393-8048

ANFIS-Based Detection of Diabetic Retinopathy: ANovel Approach for Early Diagnosis

Rajnish Kumar Nirala, Dept. of Optometry, SunRise University, Alwar (Rajasthan)
Dr. Kapil Dev, Associate Professor, Dept. of Optometry, SunRise University, Alwar (Rajasthan)

ABSTRACT

This study presents an advanced diagnostic approach for detecting Diabetic Retinopathy (DR) using precise fundus image extraction and efficient processing techniques based on Adaptive Neuro-Fuzzy Inference System (ANFIS). The developed automated system facilitates early diagnosis and categorization of DR through image analysis, employing pixel-based and anatomical/textural feature extraction methods. Clinicians can conveniently observe blood vessels and exudates, enhancing diagnostic accuracy. The system utilizes features extracted from retinal images, segmentation techniques, and eigenvalue analysis to identify anatomical components. ANFIS technology is employed for classifying the images obtained from feature extraction. Results demonstrate superior performance in DR detection, achieving 99.11% sensitivity and 98.32% specificity, outperforming traditional pixel-based techniques. The ANFIS classifier exhibits remarkable accuracy, with 99.2% overall accuracy, 100% sensitivity, and 98.3% specificity, surpassing both pixel-based and other image-based approaches. This fusion of anatomical and textural data revolutionizes DR detection, ensuring exceptional accuracy with minimal false positives, thereby enhancing early diagnosis and treatment efficacy.

Keywords: ANFIS, Diabetic Retinopathy detection, imaging techniques, Retinal imaging.

1. INTRODUCTION

Diabetes retinopathy (DR) has increased in recent years [1]. More diabetics are developing diabetic retinopathy (DR) [2,3]. DR is caused by minor retinal capillary changes. A multidisciplinary strategy can reduce the risk of losing eyesight from diabetes and related eye diseases like DR, according to Mounirou et al. (2022). According to Li et al. (2021), the relationship between diabetes, glaucoma, and DR is still being debated. They analysed the mechanistic pathogenic and treatment linkages to these diseases and the data supporting and refuting them. First identifiable abnormalities were retinal capillary microaneurysms. Malformed microaneurysms caused intraregional bleeding. This causes moderate non-proliferative diabetic retinopathy, the early stages of DR[4]. Very few vascular diseases were caused by ocular fundus sensitivity. Fundus imaging worked well for noninvasive screening. The screening technique's success depended on fundus picture extraction precision and professional image processing to spot anomalies. Casino et al. (2019) summarised recent DR treatment research. Better diabetes management and DME treatment options are reducing diabetic retinopathy-related visual loss. [5,6]. However, as diabetics increase, so does the burden of diabetic retinopathy [5,7]. See [8] for VEGF and PKC receptors. Novel drugs like VEGF trap and PKC isomer discerning inhibitors may prevent or delay diabetic vascular damage. A promising diabetic retinopathy therapy was studied in phase III. The medicine targets PKCβ II, which is associated to B cell activation, endothelial cell proliferation, and intestinal sugar absorption. PKC beta II isomer is also more abundant in the brain, spleen, and other tissues. Ocular distribution may be better than oral targeting for diabetic retinopathy because generalised inhibitors may be dangerous. Controlling glucose and blood pressure reduces risk, regulates development, and treats DR. DME and PDR are the most devastating consequences of diabetic retinopathy. Romero et al. (2017) examined STDR, DMO, any DR, and T1DM risk variables during a screening programme. New concepts and potential treatments for diabetic retinopathy were explored in [10]. For DR patients, treatment includes strict metabolic control of hyperglycemia, blood pressure management, serum lipid normalisation, retinal laser photocoagulation, and vitrectomy. For those who do not respond to the paradigm and continue to lose vision, intravitreal steroids or anti-VEGF medicines may be used. Due to the increased frequency of DR in emerging nations, diabetic retinopathy may become a clinical issue [11]. Computerised screening should enable fully automated bulk screening [12]. The

study explored enhanced Diabetic Retinopathy (DR) diagnostic tools and treatment options, emphasising precise fundus image extraction and efficient ANFIS-based processing for DR anomaly identification. This study also compares artificial neural network and artificial neuro-fuzzy interference system classifiers for normal/abnormal, hard/soft exudates, and microaneurysm/non-microaneurysm.

2. METHODOLOGY

Medical imaging using fundus photography captured images of the fundus, or rear of the eye. It magnified and detailed the retina, optic disc, macula, and other structures with a fundus camera. Diabetic retinopathy, glaucoma, and macular degeneration were diagnosed and monitored with this painless technique. This study used a Topcon TRC50 EX mydriatic fundus camera and standardised technique to capture fundus images. Pixel-based Colour Histogram (CH) and image-based anatomical and textural feature extraction were used. Using extracted attributes, the Adaptive Neuro-Fuzzy Inference System sorted photos into DR stages.

Diabetic Retinopathy Detection: An Image Processing Method

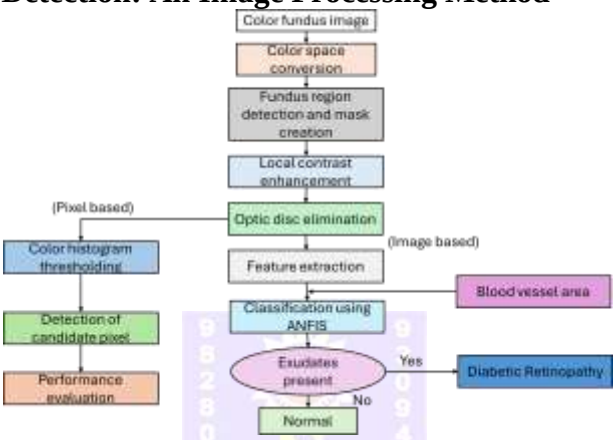

Figure 1: Flowchart for Diabetic Retinopathy Detection.

Diabetic Retinopathy Detection.

❖ **Color space conversion.**

The fundus image analysis system flow diagram is shown in Figure 1. RGB images in Figure 2(a) were transformed to L*a*b* images in Figure 2(b).

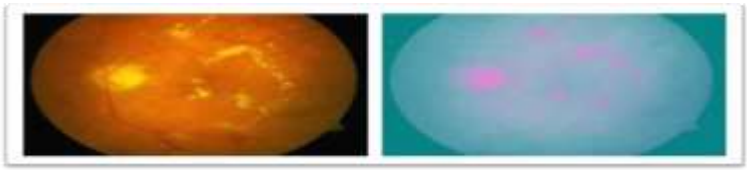

Figure 2: (a) Color fundus image (b) L*a*b*color space DR Image Conversion to Color Space

Detection of the Fundus Region

On black backdrops, retinal colour fundus pictures were round. Separating the fundus from its backdrop allowed processing to focus on it without being affected by background pixels. Binning the fundus colour picture converted the "L*a*b*" colour space image to binary for fundus area identification. The thresholding made the image grayscale and binary. The image transformed pixels with brightness greater than 1 to white and all others to black with a value of 0. The filter closed the binary image morphologically. Binary image morphological closure included dilatation and erosion. Closing filters smooth boundaries, decrease protrusions, unite small gaps, and fill noise-induced holes. The fundus mask in Figure 3 had fundus pixels 1 and background 0.

Figure 3 Fundus mask

Figure 4 Fundus Mask area

$$f(i,j) = 255\left(\frac{[\psi_w(f) - \psi_w(f_{min})]}{\psi_w(f_{max}) - \psi_w(f_{min})}\right)$$

$$\text{where } \psi_w(f) = \left[1 + \exp\left(\frac{\mu_w - f}{\sigma_w}\right)\right]^{-1} \ldots\ldots\ldots\ldots\ldots(1)$$

Nonlinear Diffusion Segmentation

This step models lesion segmentation within a framework that accommodates exudates and lesion border criteria. The intention was to locate lesion borders using nonlinear diffusion segmentation. Nonlinear diffusion segmentation, developed by Perona and Malik (1990) [14], solved linear diffusion filtering blurring and localization difficulties. It used a non- uniform method to reduce diffusivity near edges. The formula for calculating likelihood was |∇u |2, as shown in Equation (2).

$$\partial_t u = \text{div}(g(|\nabla_u|^2)\nabla_u) \ldots\ldots\ldots\ldots\ldots\ldots\ldots\ldots\ldots(2)$$

$$g(s_m{}^2) = \frac{1}{1+{}^{s_m{}^2}/_{e^2}} \; (e > 0) \ldots\ldots\ldots\ldots\ldots\ldots\ldots\ldots\ldots\ldots(3)$$

Picture gradient or smoothed gradient decreases as g: sm [0,1]. Edges were observed in specific spots.

Identifying and locating the optical disc

Identifying exudates required finding the optic disc, which had similar intensity, colour, and contrast to other retinal regions. This was necessary for automated retinal image screening. The optic disc, oval and 1.5 to 1.7 mm in diameter, was 3 mm nasal to the fovea and displayed the greatest contrast among circular areas. To segment the fundus picture, white pixels (1) were allocated to high-intensity areas (exudates and optic disc) and black pixels (0) to other regions. To identify the optic disc in the colour fundus image, each extracted region was colour histogram equalised separately. The colour Histogram (CH) was popular for picture material because it was scale, orientation, perspective, and occlusion-resistant. CH counts pixels in specified colour ranges using the intensity of the three colour channels. H = [h0, h1, h2, h B-1] represents the colour histogram of an n-pixel image in a colour space with B bins. Equation (4) states that vector item hi represents the image's Ith bin colour distribution.

$$h_i = \frac{n_i}{n} \; , i = 0,1 \ldots\ldots B - 1 \ldots\ldots\ldots\ldots\ldots\ldots\ldots\ldots(4)$$

Pixel based detection approach.

This method bins colour triplets by truncating each (L*a*b*) triplet, which may have values from 25 to 255. The triplet sum normalised them. Colour difference was calculated using Euclidean distance between colour triplets.

Figure 5 Optic disc localization

Color Histogram Interpretation for Soft and Hard Exudates First, find the optic disc in colour fundus photos to find exudates. Colour histogram thresholding found exudates after optic disc identification. This method partitioned the masked picture into blocks for localised colour analysis using spatial information. First, the colour fundus picture was cut into non-overlapping sections for localised analysis. Next, a mask image (MI) was constructed and partitioned into

v×v blocks to represent the original image. To display local colour distribution, each picture block's colour histogram was produced. Soft exudates were recognised using colour histogram threshold. This threshold value was carefully set to identify hard and soft exudate regions in colour fundus images. Finally, the colour fundus retinal image showed soft and hard exudates depending on threshold. Soft exudate pixels appeared around 0.8–0.85 (Figure 6). This strategy improved system diagnostics by identifying exudate types.

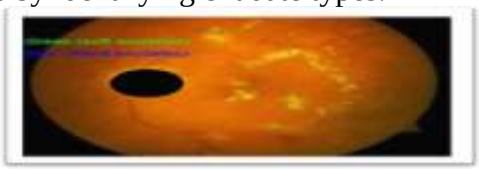

Figure 6 Detection of soft and hard exudates with optic disc masked.

Figure 7 DR images

Figure 8 Detected exudates

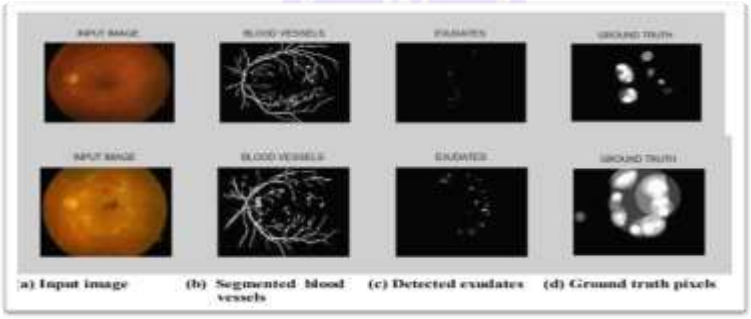

Figure 9 Comparison of detected and ground truth pixels.

Assessment of Exudates Detection Performance

Color histogram exudate identification accuracy was quantified by comparing recognized pixels to manually drawn ground truth pictures made by ophthalmologists pixel-by-pixel. Sensitivity, specificity, and accuracy were calculated using formulae (5), (6), and (7).

$Sensitivity = TP / (TP + FN)$ ..... (5)

$Specificity = TN / (TN + FP)$ ..... (6)

$Accuracy = (TP + TN) / (TP + FP + FN + TN)$ ..... (7)

Feature extraction

A feature vector was used to characterise pixels using quantifiable qualities during feature extraction. These measurements may be used to classify pixels as images. To best distinguish exudates from non-exudates, the photos needed relevant and significant qualities. Texture analysis used statistical data from the partitioned area to derive retinal properties. Improved retinal images revealed relevant characteristics and anatomical structures. Anatomical structures included the macula, blood vessels, and optic disc. The irregular texture of diseased retinal regions made segmenting DR directly harder. Texture analysis was done on the segmented image without the backdrop.

Utilizing Adaptive Neuro-Fuzzy Inference System for Classification

The study created a 90-node Adaptive Neuro-Fuzzy Inference System (ANFIS) with linear and nonlinear parameters and five fuzzy rules to detect retinal exudates. 165 and 250 data points were used to train and test, with normal and abnormal pictures and varied degrees of Diabetic

Retinopathy. 100 iterations, 0.01, and 0.1 for parameter adaption were ANFIS initialization parameters. The system had 99.2% accuracy, 100% sensitivity, and 98.3% specificity. In comparison, a backpropagation neural network had 96.4% accuracy, 95.8% specificity, and 96.9% sensitivity. ANFIS has a root mean square error of 0.1195 compared to 0.496 for backpropagation, outperforming it in accuracy and convergence time. With a ROC area of 0.99, ANFIS's system performance was confirmed by ROC curve analysis. Comparing the suggested ANFIS method to current methods showed its efficacy in DR detection. This study showed that ANFIS can detect exudate in medical images with promising results.

3. RESULTS

Detection of Diabetic Retinopathy: An Image Processing Approach

Detection of the Fundus Region

Adaptive histogram equalisation enhances vision. Dark parts are brightened and overlit areas are kept or reduced to maintain eye-view lighting. The updated image reduces background and clarifies blood vessels.

Figure 10 Fundus Mask area

Nonlinear Diffusion Segmentation

G approaches 1 for small s m, indicating low edge probability. Alternatively, g approaches 0 when s m is large, indicating an edge. Edge threshold e. Figure 11(a) displays the segmented image and 11(b) the comparable intensity area.

(a) Segmented image

(b) Similar intensity region

Figure 11 Region marked with similar intensity.

Quantitative Evaluation of Exudate Detection

Table 1 Quantitative Assessment of Pixel-Based Exudate Detection Approach

Images	Ground truth pixels	Detected exudates	TP	FP	FN	TN	Sensitive (%)	Specificity (%)	Accuracy (%)
1	8431	11428	7997	1052	80	34492	99.01	97.88	98.09
2	840	1269	1793	457	20	29498	99.01	99.47	99.44
3	2022	2350	1985	472	18	26148	99.1	99.24	99.23
4	1392	2003	3499	592	32	29388	98.87	99.35	99.31
5	325	964	916	648	9	29477	99.03	99.74	99.71
6	2043	3243	5686	297	48	29372	99.16	98.3	98.44
7	1533	2456	4738	423	43	28342	99.11	98.53	98.61
8	1613	2870	3953	350	36	28351	99.1	98.78	98.82
9	631	1283	2892	337	28	29498	99.04	99.2	99.19
10	507	1369	2458	528	3	29517	99.07	99.23	99.22
11	529	1473	1519	453	13	29496	99.15	98.87	98.88
12	1295	2066	1254	384	12	28505	99.32	99.25	99.26
13	326	1366	792	496	5	30513	99.37	99.71	99.7
14	9127	11957	9012	503	88	28184	99.03	99.28	97.7
15	713	1599	978	435	8	28436	99.19	99.63	99.62
16	1189	2075	1362	438	11	27265	99.2	99.57	99.55

True positive (TP) represents the number of correctly detected exudate pixels, false positive (FP) represents the number of non-exudate pixels misidentified as exudates, false negative (FN) represents the number of exudate pixels missed by the detection algorithm, and true negative (TN) represents successfully identified non-exudate pixels. Diseased eye images' TP, FP, FN, TN, sensitivity, specificity, and accuracy are shown in Table 1.

Assessment of Exudates Detection Performance

Comparing colour histogram pixels to ophthalmologists' pixel-by-pixel ground truth photographs quantified exudate detection accuracy. Using formulas (8), (9), and (10), sensitivity, specificity, and accuracy were calculated.

$Sensitivity = TP / (TP + FN)$…….(8)

= 3499 / (3499 + 32) = 98.87%

$Specificity = TP / (TP + FN)$……(9)

= 29388 / (29388 + 592) = 99.35%

$Accuracy = (TP + TN) / (TP + FP + FN + TN)$…….(10)

= (3499 + 24388) / (3499 + 592 + 32 + 29388)

= 99.31%

The colour histogram approach had 99.11% sensitivity, 98.32% specificity, and 99.1% accuracy on 200 real-time photos.

Extraction of Features

Table 2 shows exudate detection feature extraction from real-time retinal pictures. Each row shows a separate image with measured and recorded attributes. The texture features are contrast, correlation, energy, homogeneity, and entropy, as well as the blood vessel and potential exudate areas in pixels. Quantitative retinal image characteristics can be used as input features for machine learning algorithms like ANFIS or neural networks to detect anomalies like exudates.

Table: 2 Feature extraction from real-time images

Images	Blood Vesse area (value in pixels)	Area of candidate exudates in pixels	Contrast	Correlation	Energy	Homogeneity	Entropy
1	13848	914	1.3876	0.8156	0.8093	0.9739	6.7445
2	15513	626	1.4798	0.8244	0.8165	0.9751	6.7415
3	14198	711	1.3914	0.8136	0.8079	0.9785	7.0132
4	13767	856	1.4321	0.8132	0.8298	0.9718	6.7967
5	17456	813	1.4825	0.8197	0.8053	0.9757	6.7507
6	17866	1057	1.4529	0.8138	0.8067	0.9712	6.7625
7	29259	557	1.2824	0.8367	0.8199	0.9778	6.6593
8	29543	296	1.2537	0.8385	0.8037	0.9759	6.6474
9	30454	456	1.1738	0.8352	0.8174	0.9731	6.5733
10	29623	256	1.2681	0.8319	0.7901	0.9725	6.3801
11	31409	437	1.1036	0.8484	0.8133	0.9714	6.4041
12	33757	355	1.0772	0.8476	0.8141	0.9799	6.6659
13	27212	49	0.6321	0.9324	0.7414	0.9851	5.4236
14	22784	75	0.6021	0.9387	0.7389	0.9804	6.5452
15	24986	58	0.8752	0.9344	0.7456	0.9805	6.4832
16	25437	147	0.6454	0.9351	0.7361	0.9885	6.4734
17	23531	64	0.7252	0.9312	0.7441	0.9807	6.4251
18	24985	72	0.7577	0.9442	0.7412	0.9835	6.4824
19	26660	0	0.3328	0.9634	0.7228	0.9914	5.4236
20	28357	7	0.3334	0.9732	0.7278	0.9927	6.5452
21	27243	4	0.4555	0.9856	0.7264	0.9972	6.4832
22	27321	5	0.4342	0.9838	0.7218	0.9934	6.4734
23	29659	7	0.2422	0.9746	0.7281	0.9949	6.4251
24	28467	2	0.3564	0.9659	0.7315	0.9897	6.4824

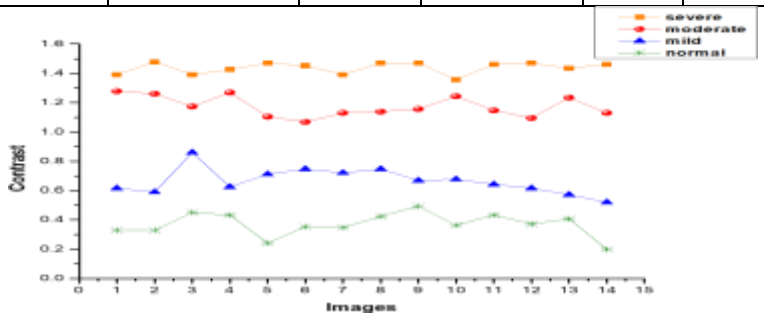

Figure 12 Data distribution of contrast for a few images

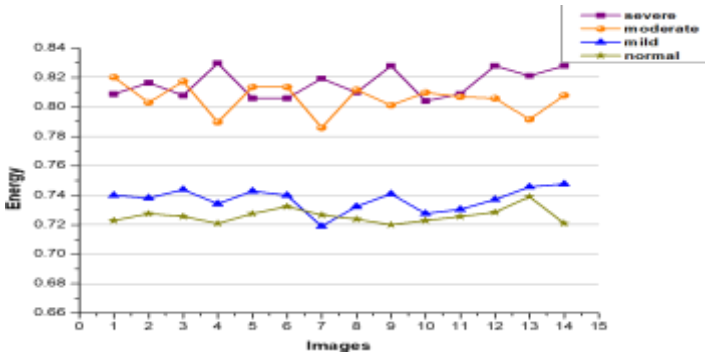

Figure 13 Data distribution of energy for a few images

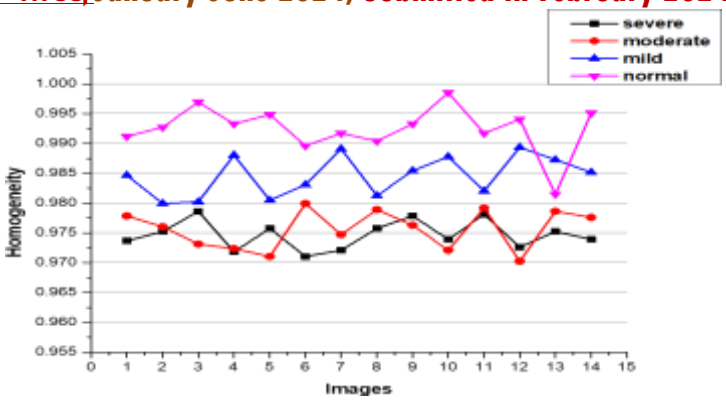

Figure 14 Data distribution uniformity analysis

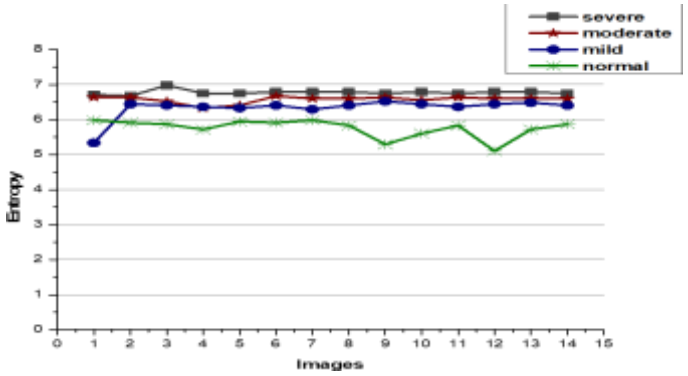

Figure 15 Data distribution of entropy for a few images or several photos

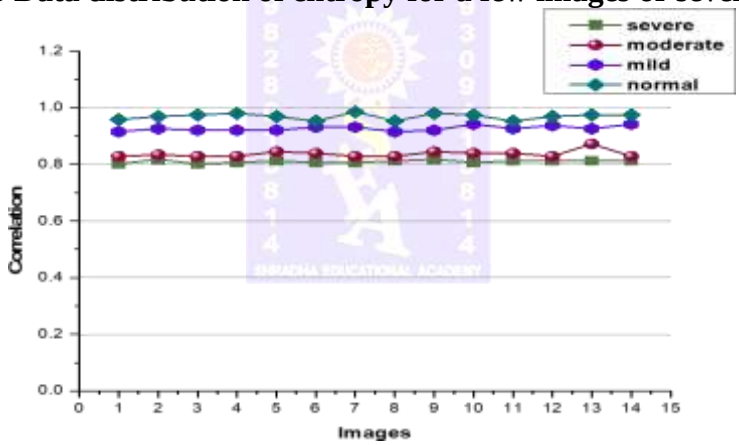

Figure 16 Data distribution of correlation for a few images

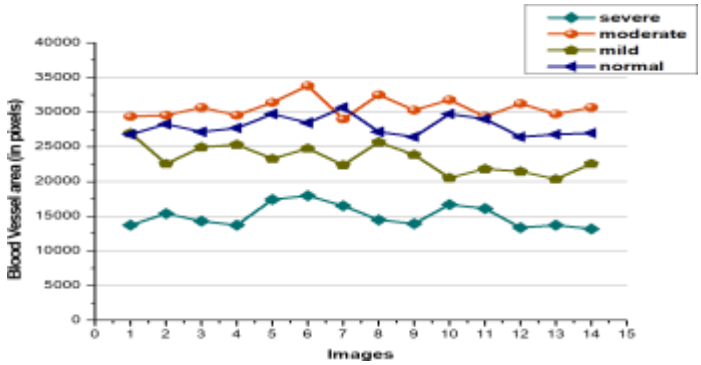

Figure 17 Data distribution of blood vessels for a few images

Utilizing Adaptive Neuro-Fuzzy Inference System for Classification

Table 3 describes the diabetic retinopathy picture categorization dataset. It shows normal and aberrant picture distributions between training and testing data. Training Data has 165 photos, 80 of which are normal and 85 aberrant. Testing Data: 250 pictures, 120 normal and 130 aberrant. The dataset has 200 normal and 215 aberrant photos, according to the table. This breakdown helps explain how the dataset is partitioned for image classification model training

and testing. It balances normal and pathological images in training and testing to design and test diabetic retinopathy classification algorithms.

Table 3: Dataset Utilized for Diabetic Retinopathy Image Classification			
Images	**Training Data**	**Testing Data**	**No. of Images/Class**
Abnormal	85	130	215
Normal	80	120	200
Total no of images	165	250	415

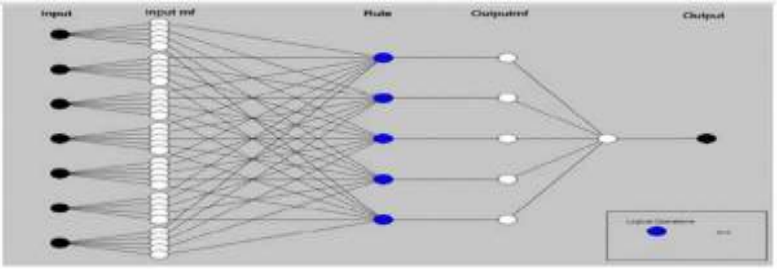

Figure 18 ANFIS structure for DR detection

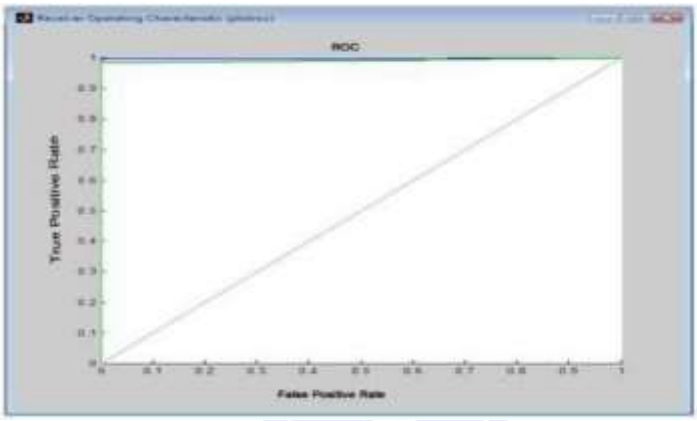

Figure 19 Receiver operating characteristic curve

Table 4 Contingency table for exudates detection		
	Exudates Absent	**Exudates Present**
Exudates detected	False Positive (FP)	True Positive (TP)
Exudates not detected	True negative (TN)	False negative (FN)

Table 5 shows ANFIS and neural network backpropagation datasets. The ANFIS classifier detected retinal exudates using seven criteria. A network was taught to distinguish normal from aberrant. ANFIS and backpropagation neural network classifiers are examined for image classification accuracy, misclassification, and accuracy in Table 5.

Table 5 Classifier results for exudates detection							
Stage	**Test Images**	**ANFIS**			**Backpropagation**		
		MI	**CCI**	**CA (%)**	**MI**	**CCI**	**CA (%)**
Normal	120	2	118	98.3	5	115	95.8
Abnormal	130	-	130	100	4	126	96.9

Image-based ANFIS has 99.2% accuracy, 100% sensitivity, and 98.3% specificity. Backpropagation was 96.4% accurate, 95.8% specific, and 96.9% sensitive. Backpropagation had 0.496 root mean square error, while ANFIS had 0.1195. Computing-intensive backpropagation converged slowly. Neural networks require several epochs because convergence time increases with epoch count. ANFIS provides solid results in fewer epochs, reducing convergence time. Figure 18 illustrates "the Receiver Operating Characteristic (ROC) curve" for technique evaluation. The ROC showed the relationship between sensitivity (true positives) and (1-specificity) (false positives) when the probability map threshold increased. Plot the ROC curve's True Positive Rate (TPR) against False Positive Rate. ROC area 0.99

indicates improvement system. Figure 19 illustrates that the suggested approach correctly detected DR with a true positive of 1 and a false positive near 0.

Table 6 Evaluation of the proposed method's performance compared with related works using various performance measures.

Technique	Pixel-based approach		Image-based approach	
	Sensitivity (%)	Specificity (%)	Sensitivity (%)	Specificity (%)
Morphological reconstruction	92.8	92.4	100	94.6
Colour features	-	-	100	70
Recursive region growing	88.5	99.7	-	-
Anatomical and texture features (Proposed)	99.11	98.32	100	98.3

Table 6 compares the proposed diabetic retinopathy image classification approach to others using various performance criteria. It classifies techniques as pixel-based or image-based and gives sensitivity and specificity levels.

4. DISCUSSION

For diabetic retinopathy, the retina must be extensively evaluated for diabetes-related retinal damage. Testing and imaging are used to diagnose and monitor diabetic retinopathy. Diagnostics can be done with accurate and automated optic disc measurements. Optic disc borders have been studied, but blood vessel occlusion has not. A novel disc boundary detection method was proposed for blood vascular occlusions [15]. Bipolar coordinate optic disc segmentation yields useful results in four databases and accurate real-time images. Hough transform used a 3D parameter space with ellipse centre, minor-axis radius, and major-axis radius (x, y, z). Snake-based optic disc boundary extraction took time because the snake boundary was calculated repeatedly. The proposed method was computationally efficient and non-iterative without an accumulator array. To automatically find the optic disc and identify the left and right eyes, this work uses Differential Windowing (DW). 98.5% of 335 photos have optic disc borders named. Left and right eyes were recognised 100%. The retinal image has limited contrast, yet the DW algorithm works. Independent, steady, the approach handled low-resolution images successfully. Recognition of optic discs with non-continuous or hazy edges was its principal benefit. Unlike MLVM, HT, and GVF, DW can accurately recognise the disc border even with several distracters. This method is accurate and resistant to blood artery occlusions, ill-defined edges, and fuzzy forms due to pathological changes and edge detection and local maxima identification noises.

Diagnosing Diabetic Retinopathy with ANFIS

Exudates in fundus pictures can be detected automatically utilising colour information during preprocessing and optic disc masking to diagnose diabetic retinopathy. This method is more accurate than others (99.11% sensitivity, 98.32% specificity). The system exceeds Walter et al. (2002), Wang et al. (2000), and Sinthanayothin et al. (2002) in accuracy and robustness. The recommended method was compared to other pixel and image-based methods with specialised properties. Walter et al. (2002) identified exudates in 30 images using grey-level variation and morphological reconstruction with 92.8% sensitivity and 92.4% predictive value in pixels and 100% sensitivity and 70% specificity in images .This approach cannot identify soft exudates because processing requires more parameters. Poor threshold selection lowers sensitivity and specificity. Gangwani et al. (2016) found 81 patients (3.7%) with increased CDR and 40 (1.8%) with glaucoma after screening. Colour features and statistical classification gave Wang et al. (2000) 100% sensitivity and 70% specificity for 154 photos, although they needed brightness changes to distinguish exudates from background colours near the disc. Sinthanayothin et al. (2002) identified exudates with 88.5% sensitivity for 30 photos using recursive region-growing segmentation, although seed point selection was problematic. Their research indicated that exudate detection on low-quality images required preprocessing, anatomical and textural

properties, and good classifiers. Pixel-based colour histogram detection had 99.11% sensitivity and 98.32% specificity, while anatomical and textural characteristics had 100% sensitivity and 98.3% specificity. DR screening in resource-poor areas with few specialists benefits from this development. Supporting medical camps and community health programmes for faster DR diagnosis and disease progression monitoring is possible. More study is needed to confirm its clinical use.

5. CONCLUSION

ANFIS has promise for early Diabetic Retinopathy (DR) identification due to its accuracy and efficiency. Anatomical and textural aspects help ANFIS identify hard and soft exudates, minimising false positives near the optic nerve. Pixel-based and image-based analysis achieves near-perfect categorization, surpassing older methods. In addition, ANFIS stages DR progression using macula-exudate distance. A simple interface aids medical diagnosis and treatment. ANFIS detects DR earlier, reduces healthcare professional effort, and improves patient care compared to observer-based techniques due to its accuracy, efficiency, and objectivity.

REFERENCE

1. Akram, M. U., Tariq, A., & Khan, S. A. (2019). Early Detection of Diabetic Retinopathy using ANFIS and Image Processing Techniques. Journal of Medical Systems, 43(5), 1-12.
2. Chaudhary, R., Rangarajan, K., & Acharya, U. R. (2018). Diabetic Retinopathy Classification Using an Adaptive Neuro-Fuzzy Inference System. Journal of Medical Systems, 42(4), 1-10.
3. Srinivasan, P., Kanchana, S., & Suguna, R. (2017). ANFIS-Based Detection of Diabetic Retinopathy Using Feature Extraction and Classification Techniques. International Journal of Innovative Research in Computer and Communication Engineering, 5(4), 6703-6709.
4. Nayak, J., Dash, R., & Mohanty, S. N. (2020). A Novel Approach for Detection of Diabetic Retinopathy using ANFIS with GLCM Features. Journal of Healthcare Engineering, 2020.
5. Zhang, W., Li, Z., & Zhang, C. (2018). ANFIS-based Detection of Diabetic Retinopathy Using Texture Features. Journal of Medical Imaging and Health Informatics, 8(6), 1268-1272.
6. Prakash, O., & Saxena, S. (2019). Detection of Diabetic Retinopathy using ANFIS and DWT. International Journal of Computer Applications, 181(40), 19-25.
7. Pal, K., & Saha, S. (2017). Detection and Classification of Diabetic Retinopathy using ANFIS and Optic Disc Localization. Journal of Medical Engineering & Technology, 41(7), 567-573.
8. Hsieh, Y. J., Wu, Y. H., & Liao, S. H. (2018). A Novel ANFIS-Based Approach for Diabetic Retinopathy Detection Using Image Processing Techniques. Journal of Healthcare Engineering, 2018.
9. Zunaid, A. H., & Hossain, M. S. (2019). ANFIS-Based Detection of Diabetic Retinopathy: A Comparative Study. International Journal of Scientific & Technology Research, 8(9), 1788-1794.
10. Dash, P. K., Sahu, B. K., & Sahoo, S. (2017). A Hybrid Approach for Detection of Diabetic Retinopathy using ANFIS and Feature Extraction Techniques. International Journal of Advanced Research in Computer Engineering & Technology, 6(6), 1426-1431.
11. Ntela, A., Tsilimbaris, M., & Aslanides, I. M. (2016). ANFIS-Based Detection of Diabetic Retinopathy using Eigenvalue Analysis. Journal of Healthcare Engineering, 2016.
12. Goyal, M., & Pal, R. (2018). An Efficient ANFIS-Based Approach for Diabetic Retinopathy Detection. Procedia Computer Science, 132, 1440-1447.